Journal Name

ARTICLE TYPE

Cite this: DOI: 10.1039/xxxxxxxxxx

Ultrafast Electron Injection to Photo-Excited Organic Molecules†

Dean Cvetko,[abc] Guido Fratesi,[d] Gregor Kladnik,[ab] Albano Cossaro,[b] Gian Paolo Brivio,[e] Latha Venkataraman,[fg] and Alberto Morgante[bh]

Received Date
Accepted Date

DOI: 10.1039/xxxxxxxxxx

www.rsc.org/journalname

Charge transfer rates at metal/organic interfaces affect the efficiencies of devices for organic based electronics and photovoltaics. A quantitative study of electron transfer rates, which take place on the femtosecond timescale, is often difficult, especially since in most systems the molecular adsorption geometry is unknown. Here, we use x-ray resonant photoemission spectroscopy to measure ultrafast charge transfer rates across the pyridine/Au(111) interfaces while also controlling the molecular orientation on the metal. We demonstrate that a bi-directional charge transfer across molecule/metal interface is enabled upon creation of a core-exciton on the molecule with a rate that has a strong dependence on the molecular adsorption angle. Through density functional theory calculations, we show that the alignment of molecular levels relative to the metal Fermi level is dramatically altered when a core-hole is created on the molecule, allowing the lowest unoccupied molecular orbital to fall partially below the metal Fermi level. We also calculate charge transfer rates as a function of molecular adsorption geometry and find a trend that agrees with the experiment. These findings thus give insight into the charge transfer dynamics of a photo-excited molecule on a metal surface.

1 Introduction

The performance of organic-based electronic devices relies on efficient charge transport across hybrid interfaces where electronically different materials couple; such interfaces often represent the bottleneck for the overall performance of organic electronic and photovoltaic devices[1]. Charge transfer (CT) across interfaces are most easily studied using small aromatic molecules that can form ordered molecular films on a variety of substrates. Often, such systems exhibit rather uniform coupling schemes to metal electrodes as well as to other molecules, therefore minimizing structural disorder, which is a major limiting factor in the device performance[2,3]. Such ordered prototypical systems open up the possibility to experimentally address charge transport phenomena on molecular level using X-ray based spectroscopy techniques[4–7].

Here we focus our study on films of pyridine molecules (PYR, C_5H_5N, inset, Fig. 1 B) formed on Au(111) surfaces with adsorption geometries that can be experimentally varied by adjusting the molecular coverage[8]. Our motivation for using this archetypical $\pi-$conjugated aromatic system is its ability to bind to Au surfaces through the formation of a weak Au-N donor-acceptor bond, with a geometry-dependent coupling, that has previously been shown to assist in charge transport through single-molecule conductance experiments[9]. In this work, we use Near Edge X-ray Absorption Fine Structure (NEXAFS), X-ray resonant photoemission (RPES) and apply core-hole-clock (CHC) analysis[4] to study electron transfer between empty molecular orbitals and the Au continuum of states in the core-excited systems. The CHC method has been used previously to determine ultrafast electron transfer times from organic molecules to underlying surfaces[6,10–15], between aromatic molecules with $\pi-\pi$ coupling[16] and also between molecules interacting through hydrogen bonding[17] as well as between donor-acceptor organic molecules[18,19].

Here, we present evidence for new core-hole decay channels present in the PYR-on-Au(111) system that reflect efficient injection of electrons *from* the Au substrate to PYR molecules on the femtosecond timescale, at a rate that depends on the orientation of the molecule on the Au substrate. We extend the stan-

[a] *Faculty of Mathematics and Physics, University of Ljubljana, Slovenia; E-mail: dean.cvetko@fmf.uni-lj.si*
[b] *CNR-IOM, Laboratorio TASC, Basovizza, Trieste, Italy*
[c] *J.Stefan Institute, Ljubljana, Slovenia.*
[d] *Dipartimento di Fisica, Università degli Studi di Milano, Italy; E-mail: guido.fratesi@unimi.it*
[e] *Dipartimento di Scienza dei Materiali, Università di Milano-Bicocca, Italy*
[f] *Department of Applied Physics, Columbia University, New York, NY; E-mail:lv2117@columbia.edu*
[g] *Department of Chemistry, Columbia University, New York, NY.*
[h] *Dipartimento di Fisica, Università di Trieste, Italy.*

† Electronic Supplementary Information (ESI) available: [details of any supplementary information available should be included here]. See DOI: 10.1039/b000000x/

dard CHC analysis to quantify the dynamics of electron injection to the molecule and find a strong dependence on the adsorption angle. The rate of electron injection from Au to the molecule increases as the molecular π system becomes flatter, enabling a greater overlap with the Au substrate, in agreement with single-molecule transport measurements[9]. Through density functional theory (DFT) calculations, we demonstrate that the core-excited lowest unoccupied molecular orbital (LUMO*) of the molecule lies partially below the Fermi level explaining the origin of the additional core-hole decay channels observed here. We also demonstrate that the coupling of the LUMO* to the Au continuum states varies with the PYR adsorption angle in agreement with the experimentally observed trends.

2 Results and Discussion

We first present results from near-edge X-ray absorption fine-structure spectroscopy (NEXAFS) for PYR films on Au(111) and use them to determine the orientation of the molecule relative to the surface[8]. We show, in Figs. 1A and 1B, NEXAFS spectra measured across the C K-edge over an energy range of 283-301 eV for a multilayer film and a monolayer film created by flash-heating a multilayer film to -55°C (see Supplemental Material for additional details on film preparation and characterization through XPS in SI Fig. S1). The main double-peak at 285 eV corresponds to a photon absorption excitation from a C1s core level to the lowest unoccupied molecular orbital (LUMO). The double-peak feature results from different C1s initial states as presented in the SI with the help of DFT based calculations for an isolated molecule. The calculated NEXAFS spectra confirm that the LUMO can be excited from both C and N sites. The LUMO of PYR has π^*-character with its nodal plane coinciding with the molecular aromatic ring[9].

We exploit the polarization dependence of the NEXAFS spectra, which are subject to dipole selection rules, to determine the molecular orientation on the surface[8]. Specifically, the C1s→LUMO transition is forbidden for light polarized in the plane of aromatic rings. We therefore determine an average angle for PYR on Au(111) by comparing the intensity of this transition with incident electric field perpendicular (p-pol) and parallel (s-pol) to the surface. For a multilayer film the intensity of the π^* excitation is independent of the electric field polarization, as can be expected for a randomly oriented molecular film[8]. In contrast, the monolayer PYR film displays a strong linear dichroism with a higher intensity peak observed in p-pol compared to s-pol. For this film, the average molecular tilt angle (θ) from the surface, determined following previously published methods[8] (see Supplemental Material) is $32^\circ \pm 3^\circ$.

In Fig. 1C, we show a series of p-pol NEXAFS spectra collected while annealing a multilayer PYR film over a temperature ranging from -106°C to -25°C. The relative intensity of the C1s→LUMO peak increases gradually with increasing temperature indicating that the molecular orientation gets flatter upon annealing. The molecular adsorption angles obtained through heating a multilayer film ranges from ∼25° to ∼65°.

We now turn to measurements of charge transfer dynamics at the PYR /Au interface by using the RPES technique and CHC anal-

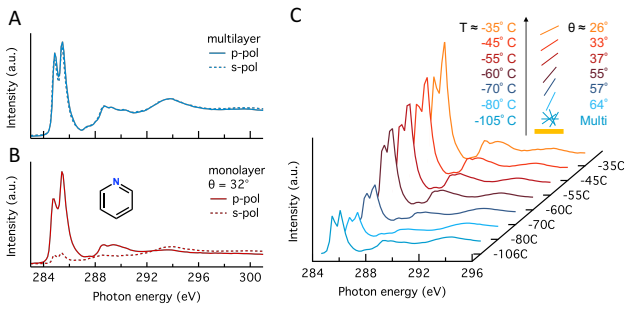

Fig. 1 C K-edge NEXAFS for (A) a PYR multilayer film taken at -106°C and (B) a monolayer film taken at -55°C. The solid (dashed) lines are measurements with light polarized perpendicular (parallel) to the Au surface. Inset: PYR structure. (C) Series of C K-edge p-pol NEXAFS spectra for a multilayer film annealed up to ~ -25°C to create monolayers with different molecular orientations. All spectra have been normalized to the intensity at 295 eV. Note that temperatures and angles are approximate.

ysis. As applied here, a core N1s electron is excited to an unoccupied molecular orbital (Fig. 2a) leaving a core-hole on the molecule. This excited state decays via three different scenarios.

In the first, known as the participator decay (Fig. 2b), the electron excited to the LUMO* de-excites in the core-hole decay with emission of an Auger electron. This leaves a single hole in one of the filled molecular orbitals and the LUMO empty. In the RPES spectrum these channels are found energetically degenerate with the respective direct photoemission from the filled molecular orbitals, i.e. HOMO-n; n=0,1,2,3, etc., but with resonantly enhanced intensity. The second, known as spectator Auger decay (Fig. 2c), involves filling the core-hole with an electron from an occupied orbital, accompanied by electron emission from another occupied orbital; this leaves the system with two holes and an additional (spectator) electron in the LUMO. Finally, when the molecule is electronically coupled to the substrate, the excited LUMO* electron can escape to the substrate, quenching both the participator and spectator decay channels and the core-hole decays via a normal Auger process (Fig. 2d). By comparing the participator decay intensity in the monolayer and multilayer systems and knowing the core-hole lifetime (5 fs for N1s and 6 fs for C1s)[20] we can determine the charge transfer times from the molecule to the substrate. However, another core-hole decay scenario arises if the LUMO* is lying below the Fermi level upon a core-hole creation (Fig. 2e). In this case, the LUMO* may get filled via electron transfer from the substrate. Thus, the characteristic spectral lines due to the decay of the LUMO* electron are observed regardless of the incident light energy[21,22]; hereafter we term this process super-participator decay.

We measure the RPES spectra, which are comprised of XPS measurements taken at a series of incident photon energies across the N K-edge of the PYR multilayer and 5 different monolayer films having PYR oriented with an angle ranging from 32° to 56°. The experimental details are given in the SI. Briefly, XPS spectra over a 50 eV kinetic energy range were measured with photon energy ($h\nu$) tuned across the N K-edge in steps of 0.1 eV (from 395 eV to 415 eV) and all spectra are presented as two-dimensional maps of intensity plotted against photon energy and electron ki-

netic energy. Fig. 2f and 2g show RPES maps for a multilayer film and a monolayer film with molecules oriented at 32°. We see strong resonances in the RPES maps at $h\nu$=399.5 eV, corresponding to an excited state decay following a N1s→LUMO* transition. These correspond to electron emission through the participator decay channel involving different occupied molecular orbitals at electron kinetic energies between 375 and 395 eV. Thus the photoemission spectrum on resonance ($h\nu$=399.5 eV) resembles that of a direct valence band photoemission (see SI Fig. S2) but with an enhanced intensity that depends on the spatial overlap of occupied orbital and the LUMO with the N1s core orbital[6].

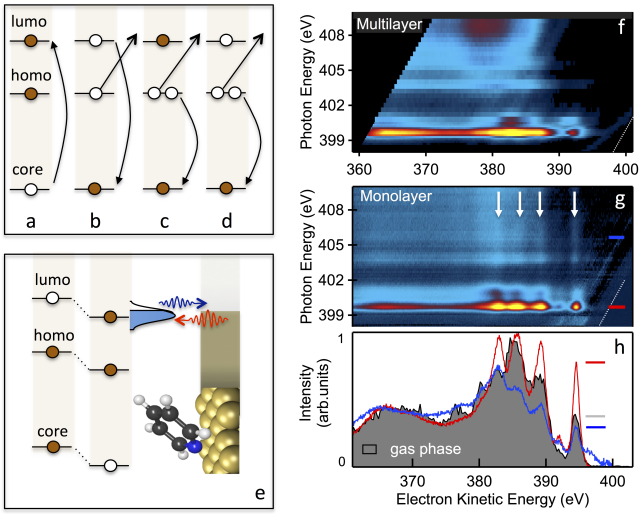

Fig. 2 Schematic of RPES process: (a) Core-hole/LUMO* excitation by X-ray absorption, (b) Participator decay, (c) Spectator decay (d) Normal Auger emission following LUMO* to substrate charge transfer. (e) Level alignment diagram following core-hole creation illustrating a bi-directional charge transfer as LUMO* is aligned at the Fermi level, leading to the super-participator signatures in RPES maps. N K-edge RPES for (f) multilayer film and (g) monolayer film oriented at 32°. The non-resonant photoemission intensity, measured below the N K-edge resonance (at $h\nu$=395 eV) has been subtracted from all spectra. Arrows indicate the super-participator peaks due to ultrafast electron injection from the Au substrate. (h) Single RPES line scans at $h\nu$=399.5 eV and 405 eV shown in red and blue, respectively. The grey shaded curve is gas phase resonant spectrum at the N1s→ LUMO excitation.

We then analyze data of the PYR monolayer with average molecular angle of 32° relative to the Au surface. The monolayer RPES map (Fig. 2g) reveals additional features, marked by the white arrows, not present in the multilayer map (Fig. 2f). These start at participator peaks in the spectrum at $h\nu$=399.5 eV, and are visible even beyond excitations to the free electron continuum above ∼ 405 eV. These features are most clearly visible in the line scans shown in Fig. 2h, where we compare data at $h\nu$=399.5 eV and at $h\nu$=405 eV with a valence band spectrum acquired for the molecule in gas phase. The clear peaks seen in the line scan taken at 405 eV (beyond the ionization edge) indicate that there are additional features that occur at constant kinetic energy. We attribute these features to the super-participator process (Fig. 2e). Once a N1s core-hole is created in PYR, the energy level alignment of all orbitals relative to the metal Fermi level is altered. The LUMO* drops at least partially below the Fermi level and may get occupied with charge from the metal as long as it is electronically well-coupled to the substrate. Thus for all incident photon energies required to create a N1s core-hole ($h\nu \geq 399.5$ eV), if an ultrafast charge injection into the LUMO* occurs within the core-hole life-time, the core-hole can decay through the super-participator channel.

Qualitatively we note that the intensity ratio of the super-participator to participator peak is large and indicative of a fast electron injection into the molecule due to a significant fraction of the LUMO* lying below the Fermi level. To quantify the charge injection rate based on the data presented in Fig. 2, we measure the participator intensity, I_p, at the LUMO* excitation ($h\nu$=399.5 eV) and the super-participator intensity above the ionization edge, I_{sp} ($h\nu$=405 eV) for PYR on Au(111) and compare them with the participator intensity at the LUMO* excitation in the gas phase, I_p^0. Details of the extended CHC analysis that use these peak intensities to determine charge transfer rates are given in the Supplemental Material document. For the PYR/Au system shown in Fig. 2 with a tilt angle of 32°, we measure $I_{sp}/I_p = 0.7 \pm 0.05$ and $I_p/I_p^0 = 0.95 \pm 0.05$. This gives for the fractional occupation of the LUMO* below Fermi $x \sim 1$, and for the electron injection time $\tau = \tau_{ch}(1 - I_{sp}/I_p)/(I_{sp}/I_p) = 3.2 \pm 0.5$ fs, where $\tau_{ch} = 5$ fs is used for the N1s core-hole lifetime[20].

We now repeat the RPES measurements and CHC analysis for four films with different molecular tilt angles ranging from 32° to 56°. The results are summarized in Fig. 3. We find that the charge injection time increases from ∼ 3.2 fs to ∼ 30 fs with increasing tilt angle of the PYR molecules. In all cases we determine the fractional occupation of the LUMO* to be close to unity ($x = 0.9 \pm 0.1$), indicating that LUMO* is filled by nearly one electron at all tilt angles of the adsorbed molecule. We also find a consistent trend of the Auger peak position above the ionization edge, passing from mostly "spectator shifted" to almost exclusively "normal Auger" for increasing tilt angles, in agreement with the observed trend in the charge injection times (details are shown in the Supplemental information). These observations imply that spatial overlap of LUMO* with the Au continuum of states is responsible for the strong angular dependence of the charge injection dynamics. We also find that ultrafast transfer of electrons from the Au occurs on both carbon and nitrogen sites of the core-excited molecule, and for both excitation sites flat lying adsorption geometries strongly enhance the rate of charge injection to the molecule.

In order to understand the role of molecular adsorption geometry on the orbital level alignment in the presence of a core-hole and on the influence of charge transfer across the organometallic interface, we turn to DFT calculations. For this work, we investigate five different molecular tilt angles: θ =0°, 30°, 45°, 60°, and 90°, and show in Fig. 4a the computed density of states (projected on the LUMO of PYR) as a function of θ, both for the ground state (blue bullets) and the N1s ionization (LUMO*, red triangles). To compare computational results with the experiment, we focus on the LUMO* case, with an added valence electron as eventually attracted from the substrate to screen the perturbation[23–27]. This corresponds to a fully relaxed electronic configuration after the molecule is ionized. The attractive potential introduced by the core hole lowers the energy of the molecular orbitals with respect

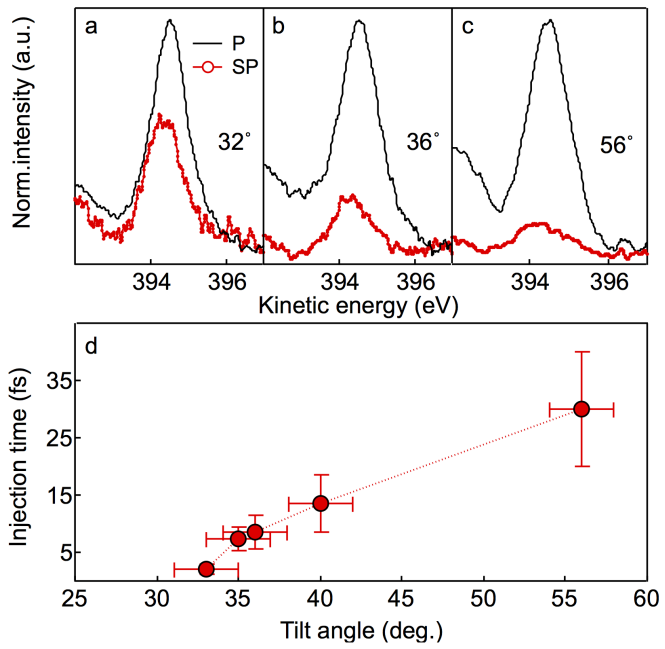

Fig. 3 Participator and super-participator peaks taken from line scans at 399.5 eV and 405 eV for PYR monolayer with tilt angle of (a) 32°, (b) 36° and (c) 56°. (d) The CT times obtained from CHC analysis of the participator and super-participator peaks as a function of molecular tilt angle.

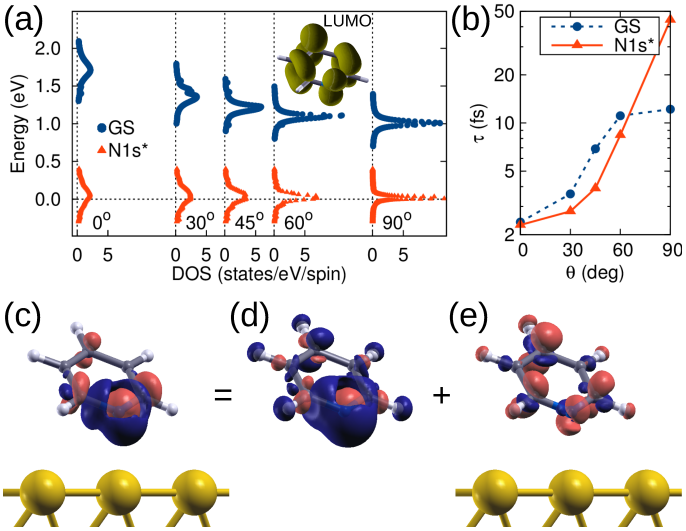

Fig. 4 (a) DFT DOS of PYR/Au(111) projected onto the LUMO of gas phase PYR (depicted in the inset) in the ground state (LUMO, bullets) and upon N1s→LUMO excitation (LUMO*, triangles). (b) Dependence of the resonant transfer time τ estimated by the LUMO/LUMO* width by a Lorentzian fit of the DOS, as a function of θ. (c) Charge displacement $\Delta\rho = \rho_{exc} - \rho_{gs}$ for $\theta = 45°$. Regions of electron accumulation and depletion are colored in bright red and dark blue, respectively. (d) The same, for an isolated molecule in the gas phase: $\Delta\rho^{(g)}$. (e) Substrate contribution $\Delta\rho'$ ($\Delta\rho = \Delta\rho^{(g)} + \Delta\rho'$). The isodensity value in panels (d-e) is 0.04 Å^{-3}.

to the ground state. The LUMO*, in particular, shows a significant fraction going below the Fermi level (see red triangles in Fig. 4a) and hence being filled by electrons from the substrate, in agreement with the experimental observations, while the ground state LUMO is always well above the Fermi level (blue bullets). The resonant transfer times for the LUMO and LUMO* are calculated from their Lorentzian width Γ, obtaining for $\theta = 45°$ $\Gamma = 95$ meV and $\Gamma = 167$ meV, *i.e.*, $\tau = 7$ fs and $\tau = 4$ fs, for the ground state and core-excited one, respectively. The difference between these values reflects the altered shape of the orbital as well the interfacial energy-level alignment upon excitation. Although the computed value is smaller than the experimental one, the agreement is remarkable given the simplicity of the theoretical model.

We now consider the effect of the molecular adsorption angle on this charge transfer time. At variance with the moderate dependence found for the ground state LUMO, the energy alignment of the LUMO* is almost independent of θ so that electron transfer from the surface is expected at all angles considered. The π symmetry of the orbital, which is depicted in the inset of Fig. 4a, is essential in determining the overlap with the substrate states and hence the dependence of τ on the angle. We observe a monotonous increase in the transfer time with θ (by a factor 3 when passing from $\theta = 30°$ to 60°), as shown in Fig. 4b, both for the values computed in the ground state and upon excitation, in agreement with the experimentally observed trend.

The electron transfer from the substrate to the ionized molecule can be visualized by evaluating the modification of the valence charge upon excitation, $\Delta\rho = \rho_{exc} - \rho_{gs}$. That is reported in Fig. 4c for $\theta = 45°$ and shows an increase of electron density in the molecular region: Mulliken population analysis[28] performed in the ground and excited states show that about 0.89 e are transfered to the molecule. A similar result was obtained at the other angles, with increased charge transfer from 0.83 e to 0.93 e when passing from $\theta = 0°$ to 90°. These values are in excellent agreement with the experimental ones (0.9 ± 0.05). The remaining charge, 0.11 e for $\theta = 45°$, can be attributed to the Au atoms in the surface layer while the bottom layers are practically unaffected (we recall that ρ_{exc} includes the added electron as provided by the metal). The electron displacement $\Delta\rho$ can be further decomposed into a molecular contribution $\Delta\rho^{(g)}$, as it would result for the ionization of free molecules in the gas phase (without the possibility of electron transfer), and a substrate contribution $\Delta\rho'$ for electron transfer and screening also accounting for the additional valence electron: $\Delta\rho = \Delta\rho^{(g)} + \Delta\rho'$. These quantities are shown in Figs. 4c, 4d and 4e, respectively. While $\Delta\rho^{(g)}$ shows in Fig. 4d a contraction of the molecular charge towards the N atom, the substrate contribution $\Delta\rho'$ in Fig. 4e highlights the filling of the LUMO* state by surface electrons. We stress that these findings follow from the specific structure of $\Delta\rho$ of the PYR /Au system and may not occur generally for organic molecules adsorbed on metals. For example, a similar alignment of LUMO* to the Fermi level was computed for pyridine on graphene[27], but complete filling of LUMO* for pentacene/Al(001) has been evaluated and observed[24,26].

3 Conclusions

We explored the dynamics of charge transfer in a series of PYR/Au(111) layers with different adsorption angles, and find

that the LUMO* of the core excited molecules falls partially below the Au Fermi level, opening a gateway for ultrafast injection of electrons from gold substrate to the molecule. Importantly, we have extended the standard CHC analysis of the RPES spectra to determine this charge transfer rate and show that it depends on the orientation of the molecule to the metal surface; the flatter molecules have a significantly faster charge transfer. Through DFT calculations, we show that the core-excited PYR/Au has a LUMO* that lies partially below Fermi, with an excellent agreement between computed occupation values and best-fit results from the measurements. We also find that the broadening of this orbital due to its electronic coupling to the Au continuum of states enables an ultrafast charge transfer from the Au to the molecule within the core-hole life time. We further calculate the angular dependence of the charge injection rate and find a trend consistent with the experiment of faster dynamics for flatter lying molecules. These findings have a direct consequence on understanding the mechanism of charge transfer at molecular junctions for hetero-organic photovoltaics, where alignment of donor and acceptor orbitals in the presence of a valence exciton dictates the efficiency of exciton dissociation, charge separation, and consequently device performance.

4 Methods

Condensed phase and gas phase measurements have been performed at the ALOISA and ANCHOR beamlines of the Elettra synchrotron in Trieste, Italy[29]. Au(111) substrate was prepared by cycles of Ar^+ ion sputtering and temperature annealing. Pyridine molecules were vacuum deposited on the Au substrate through a leak valve operated in $\sim 10^{-7}$mbar pressure range. PYR multilayer was grown with the sample held below 200 K, whereas monolayer phases with variable adsorption geometry were produced by temperature annealing of multilayer films up to T$\sim$250K. NEXAFS at Nitrogen (Carbon) K-edge was performed by collecting emission of secondary electrons as partial absorption yield with high pass filter set to 370 eV (250 eV). All NEXAFS were measured with linear photon polarization in *s-pol* geometry (electric field vector $\vec{E}$ parallel to the surface plane), *p-pol* geometry ($\vec{E}$ along the surface normal) or at magic angle (angle between $\vec{E}$ and surface normal 54.7°). Photoemission experiments were performed with electron analyzer positioned along the photon polarization $\vec{E}$. Photon energy of hν=650, 500, and 130 eV was used for core-level and valence band spectra, with an overall energy resolution of $\sim$ 100 meV. RPES at N (C) K-edge was conducted by taking a series of XPS scans with photon energy between 395-425 eV (280-310 eV) in steps of 0.1-0.2 eV. For each photon energy, XPS spectrum covering $\sim$60 eV kinetic energy (E_k) range was measured to construct a two-dimensional like RPES map I(hν,E_k). The non-resonant spectra were measured in the pre-edge region with photon energy of 395 eV (283 eV), and were subtracted from each XPS spectrum in the RPES maps I(hν,E_k). Participator intensity was evaluated after normalization to the integrated Auger, from the integrated intensities of the upper valence peaks (e.g. HOMO in the 0-8 eV binding energy range). Super-participator intensity was evaluated from the XPS spectra with photon energy above the ionization edge, h$\nu > 405$eV (h$\nu >$ 292eV) as integrated intensity in the fixed kinetic energy range ($\sim$380 eV), containing the electron emission from HOMO. More details about the spectra acquisition conditions, the preparation of the sample, and the implementation of the CHC method are given in the Supplemental Material.

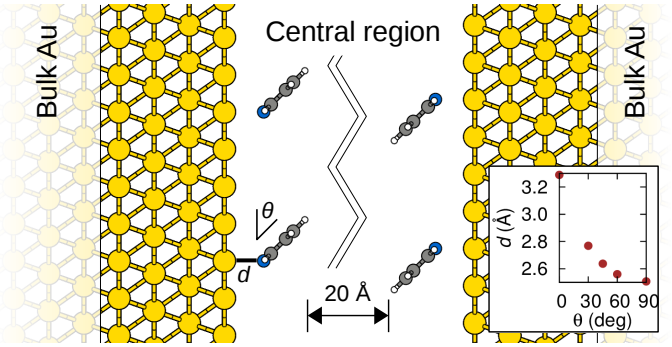

Fig. 5 Structural setup for computing the electronic structure of PYR adsorbed on semi-infinite Au(111). The inset shows the dependence of the N-Au distance d on the angle θ as determined in Ref.[35].

We use the SIESTA/TranSIESTA simulation packages[30,31] with the Perdew, Burke, and Ernzerhof (PBE) exchange-correlation functional[32]. To obtain a detailed analysis of the coupling between the PYR molecule and the substrate, especially to deal with the lineshapes of the resonant orbitals, it is most convenient to consider a continuum of Au states. We adopt a description derived from electron transport[31] where a semi-infinite substrate is taken into account by a Green's function approach[33,34]. For computational convenience we replicate the system and model two facing semi-infinite Au substrates, each having a PYR molecular layer. Facing molecules are separated by at least 20 Å to prevent any interaction between the two sides (see Fig. 5). Periodic boundary conditions in the lateral directions are taken within a 4×4 Au surface unit cell (coverage fixed to 1/16).

In describing the angle-dependent properties, we adopt the molecular adsorption geometry on the Au(111) surface from the work of Mollenhauer et al,[35], with the PYR N atom on the a-top site on the Au surface and an Au-N distance that depends on the molecular tilt angle. Such a dependence was determined by structural optimizations within DFT corrected for van der Waals interactions, and is summarized in the inset of Fig. 5. To describe the case of a molecule excited by X-ray radiation, we promote a N1s electron from the core to a valence state. The core-hole is included in the pseudopotential that accounts for the interaction of valence electrons with a core-excited N1s* ion. The resonant electron/hole injection time τ from the LUMO is then determined as $\tau = \hbar/\Gamma$[36,37] from the Lorentzian full width at half-maximum (FWHM) Γ in the density of states projected onto the LUMO:

$$\rho_\Phi(E) = \frac{1}{\pi}\mathrm{Im}\left[G_{\Phi\Phi}(E)\right] \propto \frac{1}{\pi}\frac{(\Gamma+\gamma)/2}{(E-E_\Phi)^2+[(\Gamma+\gamma)/2]^2}. \qquad (1)$$

Here, the LUMO energy E_Φ and width Γ are fitting parameters, $G_{\Phi\Phi}(E)$ is the expectation value of the Green's function on the Φ state, and $\gamma = 4$ meV an additional broadening added for computational convenience.

5 Acknowledgements

Authors greatly acknowledge fruitful discussions with A.Batra and O.Adak. We acknowledge support from the MIUR of Italy through PRIN projects (no. 20104XET32, 20105ZZTSE), and ANCHOR project of the FIRB 2010 call (ref. RBFR10FQBL), and MAE project (US14GR12). Part of this research was also funded through *Progetto Premiale 2012 ABNANOTECH*. Computational resources are made available in part by CINECA (application codes HP10C0TP0R and HP10CESYLM). DC and GK acknowledge support from the Slovenian Research Agency (Project no. P1-0112 and Z1-6726). LV thanks the Packard Foundation for support.

References

1 S. R. Forrest, *Nature*, 2004, **428**, 911–918.

2 F. Schreiber, *Progress in Surface Science*, 2000, **65**, 151–257.

3 J. V. Barth, *Annual Review of Physical Chemistry*, 2007, **58**, 375–407.

4 P. A. Brühwiler, O. Karis and N. Mårtensson, *Reviews of Modern Physics*, 2002, **74**, 703–740.

5 D. Menzel, *Chemical Society reviews*, 2008, **37**, 2212–2223.

6 P. Vilmercati, D. Cvetko, A. Cossaro and A. Morgante, *Surface Science*, 2009, **603**, 1542–1556.

7 L. Cao, X.-Y. Gao, A. T. S. Wee and D.-C. Qi, *Advanced Materials*, 2014, **26**, 7880–7888.

8 J. Stöhr, *NEXAFS Spectroscopy*, Springer Berlin Heidelberg, Berlin, Heidelberg, 1992, vol. 25.

9 S. Y. Quek, M. Kamenetska, M. L. Steigerwald, H. J. Choi, S. G. Louie, M. S. Hybertsen, J. B. Neaton and L. Venkataraman, *Nature Nanotechnology*, 2009, **4**, 230–234.

10 L. Cao, Y.-Z. Wang, T.-X. Chen, W.-H. Zhang, X.-J. Yu, K. Ibrahim, J.-O. Wang, H.-J. Qian, F.-Q. Xu, D.-C. Qi and A. T. S. Wee, *The Journal of Chemical Physics*, 2011, **135**, 174701.

11 L. Cao, Y. Wang, J.-q. Zhong, Y.-Y. Han, W. Zhang, X. Yu, F. Xu, D. Qi and A. T. S. Wee, *The Journal of Physical Chemistry C*, 2014, **118**, 4160–4166.

12 G. Kladnik, D. Cvetko, A. Batra, M. DellâĂŹAngela, A. Cossaro, M. Kamenetska, L. Venkataraman and A. Morgante, *The Journal of Physical Chemistry C*, 2013, **117**, 16477–16482.

13 J. Schnadt, P. A. Brühwiler, L. Patthey, J. N. O'Shea, S. Södergren, M. Odelius, R. Ahuja, O. Karis, M. Bässler, P. Persson, H. Siegbahn, S. Lunell and N. Mårtensson, *Nature*, 2002, **418**, 620–623.

14 F. Blobner, P. B. Coto, F. Allegretti, M. Bockstedte, O. Rubio-Pons, H. Wang, D. L. Allara, M. Zharnikov, M. Thoss and P. Feulner, *The Journal of Physical Chemistry Letters*, 2012, **3**, 436–440.

15 O. Adak, G. Kladnik, G. Bavdek, A. Cossaro, A. Morgante, D. Cvetko and L. Venkataraman, *Nano Letters*, 2015, **15**, 8316–8321.

16 A. Batra, G. Kladnik, H. Vázquez, J. S. Meisner, L. Floreano, C. Nuckolls, D. Cvetko, A. Morgante and L. Venkataraman, *Nature Communications*, 2012, **3**, 1086.

17 G. Kladnik, M. Puppin, M. Coreno, M. de Simone, L. Floreano, A. Verdini, A. Morgante, D. Cvetko and A. Cossaro, *Nano Letters*, 2016, **16**, 1955–1959.

18 P. Vilmercati, C. Castellarin-Cudia, R. Gebauer, P. Ghosh, S. Lizzit, L. Petaccia, C. Cepek, R. Larciprete, A. Verdini, L. Floreano, A. Morgante and A. Goldoni, *Journal of the American Chemical Society*, 2009, **131**, 644–652.

19 T. Schiros, G. Kladnik, D. Prezzi, A. Ferretti, G. Olivieri, A. Cossaro, L. Floreano, A. Verdini, C. Schenck, M. Cox, A. a. Gorodetsky, K. Plunkett, D. Delongchamp, C. Nuckolls, A. Morgante, D. Cvetko and I. Kymissis, *Advanced Energy Materials*, 2013, **3**, 894–902.

20 M. Coville and T. D. Thomas, *Physical Review A*, 1991, **43**, 6053–6056.

21 A. J. Britton, A. Rienzo, J. N. O'Shea and K. Schulte, *The Journal of chemical physics*, 2010, **133**, 094705.

22 C. Sauer, M. Wießner, A. Schöll, F. Reinert, M. WieBner, A. Schöll and F. Reinert, *Materials Science*, 2013, **17**, 1–5.

23 S. García-Gil, A. García and P. Ordejón, *The European Physical Journal B*, 2012, **85**, 239.

24 A. Baby, G. Fratesi, S. R. Vaidya, L. L. Patera, C. Africh, L. Floreano and G. P. Brivio, *The Journal of Physical Chemistry C*, 2015, **119**, 3624–3633.

25 T. Susi, D. J. Mowbray, M. P. Ljungberg and P. Ayala, *Phys. Rev. B*, 2015, **91**, 081401.

26 A. Baby, H. Lin, G. P. Brivio, L. Floreano and G. Fratesi, *Beilstein J. Nanotechnol.*, 2015, **6**, 2242Ð2251.

27 A. Ravikumar, A. Baby, H. Lin, G. P. Brivio and G. Fratesi, *Sci. Rep.*, 2016, **6**, 24603.

28 R. S. Mulliken, *Journal of Chemical Physics*, 1955, **23**, 1833–1840.

29 L. Floreano, G. Naletto, D. Cvetko, R. Gotter, M. Malvezzi, L. Marassi, A. Morgante, A. Santaniello, A. Verdini, F. Tommasini and G. Tondello, *Review of Scientific Instruments*, 1999, **70**, 3855.

30 J. M. Soler, E. Artacho, J. D. Gale, A. García, J. Junquera, P. Ordejón and D. Sánchez-Portal, *Journal of Physics: Condensed Matter*, 2002, **14**, 2745–2779.

31 M. Brandbyge, J.-L. Mozos, P. Ordejón, J. Taylor, K. Stokbro and P. Ordejo, *Physical Review B*, 2002, **65**, 1–17.

32 J. P. Perdew, K. Burke and M. Ernzerhof, *Physical Review Letters*, 1996, **77**, 3865–3868.

33 D. Sánchez-Portal, D. Menzel and P. M. Echenique, *Physical Review B*, 2007, **76**, 235406.

34 G. Fratesi, C. Motta, M. I. Trioni, G. P. Brivio and D. Sánchez-Portal, *The Journal of Physical Chemistry C*, 2014, **118**, 8775–8782.

35 D. Mollenhauer, N. Gaston, E. Voloshina and B. Paulus, *Journal of Physical Chemistry C*, 2013, **117**, 4470–4479.

36 S. Datta, *Quantum Transport - Atom to Transistor*, Cambridge University Press, 2005.

37 A. Nitzan, *Chemical Dynamics in Condensed Phases: Relaxation, Transfer and Reactions in Condensed Molecular Systems*, Oxford University Press, 2006.